Acceleration of a focused plasma jet in a divergent magnetic nozzle

IEPC-2009-002

Presented at the 31st International Electric Propulsion Conference,
University of Michigan, Ann Arbor, Michigan, USA
September 20–24, 2009

E. Ahedo * and M. Merino †
Universidad Politécnica de Madrid, 28040 Madrid, Spain

A two dimensional model of a divergent magnetic nozzle is used to analyze the conversion of thermal into kinetic energy for a collisionless plasma jet with a large radial density gradient at the nozzle entrance. Comparisons with a 1D model and with a uniform plasma jet are made. The focused plasma jet has a much better nozzle efficiency. The large Hall current required to focus the jet increases downstream and sets up two magnetic detachment mechanisms: an induced magnetic field and azimuthal electron inertia effects. This second mechanism seems stronger than the first one.

I. Introduction

A divergent magnetic nozzle is used to accelerate a magnetized plasma in the applied-field magnetoplasmadynamic (MPD) thruster,[1] the helicon thruster,[2] the VASIMR,[3] and the diverging cusped field thruster (DCFT).[4] Andersen et al.[5] showed the analogy between the dynamics of a magnetized plasma in a magnetic nozzle and a neutral gas in a solid (deLaval) nozzle: the plasma flow is tied to the magnetic streamlines and a regular sonic transition occurs at the magnetic throat, i.e. the radial section where the magnetic field is maximum. However, plasma dynamics in a magnetic nozzle are more complex than gas dynamics in a solid nozzle. For instance: there are several possible sources of plasma 'internal' energy; Lorentz forces compete with thermal pressure; the plasma can be put into rotation; self-magnetic fields can be induced; the response changes with plasma collisionality and ion magnetization. In addition, once the plasma is accelerated the plasma must detach (via inertia, resistivity, or induced magnetic field) from the turning magnetic lines in order to achieve the desired axial thrust.[6–8]

We have presented recently a two-dimensional (2D) model of the acceleration of a current-free plasma in a divergent magnetic nozzle with fully magnetic-guided electrons.[9] Ion momentum is gained from the electron thermal pressure, via the electrostatic self-field. It was shown that except for unusually large magnetic fields, ion magnetization is weak and ion streamlines deviate from magnetic (i.e. electron) streamlines. As a consequence the local ambipolar condition does not hold, and local electric currents are formed. The model takes into consideration both azimuthal ion and electron currents, but simulations in that paper were limited to one magnetic nozzle profile and a uniform non-rotating plasma jet at the entrance. Notice that both the *upstream* subsonic region (in a convergent nozzle or inside a plasma device), where the plasma is generated and heated, and the *downstream* detachment region are out of the scope of the supersonic acceleration model. The upstream subsonic condition is treated in a separate paper.[10]

The main goal of this paper is to analyze the acceleration of a collisionless plasma jet with a large radial gradient of the plasma density. This plasma configuration can be found at the exit of a dielectric cylindrical vessel with a parallel magnetic field.[10] The density gradient is balanced by the magnetic confinement force created by a large Hall-current (i.e. the electron azimuthal drift). The differences in behavior between the focused and the uniform plasma jet will be discussed. Finally, an assessment of magnetic detachment mechanisms will be made.

*Professor. E-mail: eduardo.ahedo@upm.es. Full address: E.T.S. Ingenieros Aeronáuticos, Plaza Cardenal Cisneros, Madrid 28040.
†MSc Student.

II. Model formulation

The plasma-nozzle model was presented in Ref. 9. A summary is given here. A collisionless plasma is flowing in a guiding, longitudinal magnetic field, $\boldsymbol{B} = B_r\mathbf{1}_r + B_z\mathbf{1}_z$. The cylindrical and magnetic reference frames are $\{\mathbf{1}_z, \mathbf{1}_r, \mathbf{1}_\theta\}$ and $\{\boldsymbol{b}, \mathbf{1}_\perp, \mathbf{1}_\theta\}$, with $\boldsymbol{b} = \boldsymbol{B}/B = \cos\alpha\mathbf{1}_z + \sin\alpha\mathbf{1}_r$, and $\mathbf{1}_\perp = -\sin\alpha\mathbf{1}_z + \cos\alpha\mathbf{1}_r$. The solenoidal magnetic field admits the magnetic streamfunction $\psi(r,z)$, with

$$\nabla\psi = rB\mathbf{1}_\perp : \quad rB_r = -\partial\psi/\partial z, \quad rB_z = \partial\psi/\partial r. \tag{1}$$

The magnetic flux across a section $z = z_c,\ 0 \le r \le r_c$, is

$$2\pi\int_0^{r_c} B_z r dr = 2\pi\psi(r_c, z_c).$$

Results here are presented for the magnetic field created by a current ring placed at $z = 0$ and of radius R_L. Then, the magnetic streamfunction is[11]

$$\psi(r,z) = \frac{2B_0R_L^2 r}{\pi}\cdot\frac{\left(2-k^2\right)\mathbf{K}\left(k^2\right) - 2\mathbf{E}\left(k^2\right)}{k^2\sqrt{\left(R_L+r\right)^2+z^2}}, \tag{2}$$

with $k^2 = 4R_Lr/(R_L+r)^2+z^2$, $B_0 = B_z(0,0)$, and $\mathbf{K}(m)$ and $\mathbf{E}(m)$ the complete elliptic integrals of first and second kind, respectively, with the argument m as defined by Abramowitz and Stegun.[12] Figure 1 plots this magnetic topology.

A plasma jet is injected sonically at the nozzle throat, at $z = 0$, and is accelerated supersonically in the divergent nozzle. The steady-state, axisymmetric (i.e. $\partial/\partial\theta = 0$) response is considered. Plasma quasineutrality holds (i.e. $n_e = n_i = n$), all collisional effects are neglected, and electric currents in the plasma are assumed small enough to neglect the induced magnetic field. Electron inertia is disregarded (i.e. $m_e/m_i \to 0$) and the magnetic field is strong enough to guide electrons. This restricts electron motion, which can include an azimuthal drift, to magnetic streamsurfaces. Let R, with $R < R_L$, be the radius of the plasma jet at the throat A of the magnetic nozzle. Then, magnetic guiding of electrons and plasma quasineutrality yield that the magnetic streamsurface V: $r = R_V(z)$, with $R_V(z)$ defined implicitly by $\psi(R_V(z), z) = \psi(R, 0)$, contains the whole plasma jet. Although the magnetic streamsurface $r = R_V(z)$ is containing the external ion streamsurface, the model deals with any degree of ion magnetization. Except for strong ion magnetization, the ion streamsurfaces are not contained in general in magnetic streamsurfaces. Observe that the ratio R/R_L measures the divergence rate of the magnetic nozzle acting on the plasma jet. Figure 1 shows the boundaries of the two plasma jets simulated in Ref. 9 and here.

For vectorial quantities it is convenient to distinguish the longitudinal (vectorial) component with a tilde. For instance, the ion velocity is expressed as $\boldsymbol{u}_i = \tilde{\boldsymbol{u}}_i + u_{\theta i}\mathbf{1}_\theta$. Thus, the ion continuity equation is

$$\nabla\cdot n\boldsymbol{u}_i = \nabla\cdot n\tilde{\boldsymbol{u}}_i = 0, \tag{3}$$

and $\tilde{\boldsymbol{u}}_i$ admits a streamfunction, ψ_i, satisfying $rnu_{ri} = -\partial\psi_i/\partial z$ and $rnu_{zi} = \partial\psi_i/\partial r$. The longitudinal and azimuthal ion momentum equations lead to[9]

$$m_i\tilde{\boldsymbol{u}}_i\cdot\nabla\tilde{\boldsymbol{u}}_i = -e\nabla\phi + eu_{\theta i}\mathbf{1}_\theta\times\boldsymbol{B} + \mathbf{1}_r m_i u_{\theta i}^2/r \tag{4}$$

$$rm_iu_{\theta i} + e\psi = D_i(\psi_i), \tag{5}$$

with $D_i(\psi_i)$ determined from entrance conditions. The projection of Eq. (4) along the ion streamlines yields the conservation of the ion mechanical energy,

$$e\phi + m_iu_i^2/2 = H_i(\psi_i).$$

The zero electron-inertia limit yields $\tilde{\boldsymbol{u}}_e = u_{\parallel e}\boldsymbol{b}$. An isothermal electron model is assumed: except for the small electron current flowing downstream and neutralizing the ion current, electrons are confined and occasional collisions tend ultimately to thermalize it. Then, the applicable electron equations are[9]

$$nu_{\parallel e}/B = G_e(\psi), \tag{6}$$

$$0 = -T_e\nabla n + en\nabla\phi - enu_{\theta e}B\mathbf{1}_\perp, \tag{7}$$

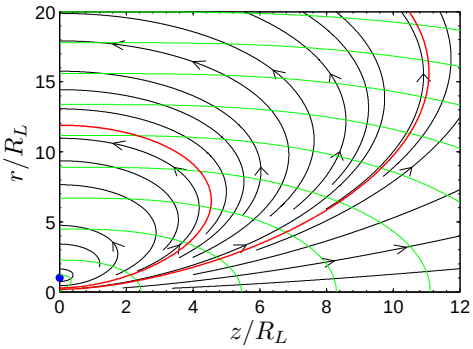

Figure 1. Black lines are the magnetic streamlines created by a circular ring located at $r = R_L$, $z = 0$. Green lines are the constant-B lines. The two red lines correspond to the two plasma jets used in the simulations.

with $G_e(\psi)$ the electron-to-magnetic flux ratio. The vectorial force balance decomposes into

$$T_e \ln n - e\phi = H_e(\psi), \tag{8}$$

$$u_{\theta e} = -\frac{1}{eB}\frac{\partial H_e}{\partial \mathbf{1}_\perp} = -\frac{r}{e}\frac{dH_e}{d\psi}, \tag{9}$$

where $T_e \ln n$ is the (specific) enthalpy of the electron gas, and $H_e(\psi)$ is the total (specific) enthalpy. Both $G_e(\psi)$ and $H_e(\psi)$ are determined from entrance conditions.

In each streamsurface, Eq. (8) can be interpreted as either the conservation of total enthalphy or the Maxwell-Boltzmann equilibrium (with $-H_e/e$ the thermalized potential). Equation (9) shows that the electron azimuthal velocity is a B-perpendicular drift, with contributions of both the electric field and the pressure gradient. More important is that Eq. (9) states that the ratio $u_{\theta e}/r$ remains constant in each streamsurface. As a consequence, if the electron azimuthal drift is zero at the entrance, it remains zero in the whole nozzle; if it is not zero, it increases with the radius of the corresponding magnetic streamsurface.

Substituting the electric potential from Eq. (8), Eqs. (3) and (**??**) become

$$u_{ri}\frac{\partial \ln n}{\partial r} + u_{zi}\frac{\partial \ln n}{\partial z} + \frac{\partial u_{ri}}{\partial r} + \frac{\partial u_{zi}}{\partial z} = -\frac{u_{ri}}{r}, \tag{10}$$

$$u_{ri}\frac{\partial u_{ri}}{\partial r} + u_{zi}\frac{\partial u_{ri}}{\partial z} + c_s^2\frac{\partial \ln n}{\partial r} = (u_{\theta i} - u_{\theta e})\Omega_i \cos\alpha + \frac{u_{\theta i}^2}{r}, \tag{11}$$

$$u_{ri}\frac{\partial u_{zi}}{\partial r} + u_{zi}\frac{\partial u_{zi}}{\partial z} + c_s^2\frac{\partial \ln n}{\partial z} = -(u_{\theta i} - u_{\theta e})\Omega_i \sin\alpha, \tag{12}$$

where $c_s = \sqrt{T_e/m_i}$ is the plasma sound speed and $\Omega_i(r,z) = eB/m_i$ is the *local* ion gyrofrequency.

Boundary conditions yield plasma magnitudes at the magnetic throat. These determine the ion stream-function at the entrance, $\psi_i(r,0)$, and functions $D_i(\psi_i)$, $H_i(\psi_i)$, $H_e(\psi)$, and $G_e(\psi)$. Then, the method of characteristics[13] is used to integrate Eqs. (10)-(12) for n, u_{zi}, and u_{ri}. The families of characteristic curves are the ion streamlines and the pair of Mach lines. The numerical integration stops at a certain section, $z = z_F$, located before the turning section, $dr/dz|_V \to \infty$, of the magnetic tube V. The rest of plasma variables (ϕ, $u_{\theta i}$, $u_{\theta e}$, and $u_{\parallel e}$) are determined from algebraic conservation equations. Other magnitudes of interest are the ion and electron density currents, $\boldsymbol{j}_i = en\boldsymbol{u}_i$ and $\boldsymbol{j}_e = en\boldsymbol{u}_e$ (notice the sign used in j_e), and the electron current density

$$\boldsymbol{j} \equiv \tilde{\boldsymbol{j}} + j_\theta \mathbf{1}_\theta = \boldsymbol{j}_i - \boldsymbol{j}_e. \tag{13}$$

Prior to integration, magnitudes are non-dimensionalized with the energy T_e, the velocity c_s, the length R, the density $n_0 = n(0,0)$, the electric current density $j_0 = en_0c_s$, and so on. Dimensionless variables are expressed with a hat, e.g. $\hat{u} = u/c_s$. Since the plasma is isothermal $\hat{u}_i$ is the Mach number M too. Just for reference, Table 1 gives typical magnitudes at the magnetic throat for a small and a large plasma source.

	Low-power plasma	High-power plasma
magnetic field at entrance, B_0	0.1T	1T
plasma density at entrance, n_0	$10^{18}\mathrm{m}^{-3}$	$2\cdot 10^{19}\mathrm{m}^{-3}$
electron temperature, T_e	10eV	40eV
nozzle throat radius, R	$2\cdot 10^{-2}$m	10^{-1}m
thermal velocity, c_e	$1.3\cdot 10^{6}$m/s	$2.7\cdot 10^{6}$m/s
sound velocity, c_s	$4.9\cdot 10^{3}$m/s	$9.8\cdot 10^{3}$m/s
Alfven velocity, c_A	$3.4\cdot 10^{5}$m/s	$7.7\cdot 10^{5}$m/s
Debye length, λ_d	$2.4\cdot 10^{-5}$m	$1.1\cdot 10^{-5}$m
electron Larmor radius, l_e	$7.5\cdot 10^{-5}$m	$1.5\cdot 10^{-5}$m
ion Larmor radius, l_i	$2.0\cdot 10^{-2}$m	$2.0\cdot 10^{-3}$m
ion gyrofrequency, Ω_i	$2.4\cdot 10^{5}\mathrm{s}^{-1}$	$2.4\cdot 10^{6}\mathrm{s}^{-1}$
ion current, I_i	1A	1000A
quasineutrality parameter, λ_D/R	$1.2\cdot 10^{-3}$	$1.1\cdot 10^{-4}$
magnetic guiding parameter, ℓ_e/R	$3.7\cdot 10^{-3}$	$1.5\cdot 10^{-4}$
magnetic detachment parameter, $S_m(0)$	$2.5\cdot 10^{-4}$	$2\cdot 10^{-4}$
inertial detachment parameter, $S_i(0)$	$7.5\cdot 10^{-3}$	$3\cdot 10^{-4}$

Table 1. Typical parameters at the nozzle throat for a low-power(L) and a high-power(H) plasma source.

III. Acceleration of a uniform plasma jet

Let us consider first the simplest case of a plasma jet that, at the entrance, is uniform, current-free, with no swirling (i.e. ion rotation) and no Hall current. Thus, boundary conditions at $z=0$ are

$$\hat{u}_{ri}=0,\quad \hat{u}_{\theta i}=0,\quad \hat{u}_{zi}=M_0, \tag{14}$$

$$\hat{u}_{re}=0\quad \hat{u}_{ze}=M_0, \tag{15}$$

$$\hat{\phi}=0,\quad \hat{n}=1,\quad \hat{u}_{\theta e}=0, \tag{16}$$

with $M_0\geq 1$ the plasma Mach number at the entrance, which is set at 1.05 ($M_0=1$ is not accepted by the integration scheme, but the solution is not very sensitive to M_0-1). The dimensionless parameters of the problem are the nozzle divergence rate, measured by R/R_L, and the ion magnetization strength, $\hat{\Omega}_{i0}=eB_0R/m_ic_s\equiv R/\ell_{i0}$, with ℓ_{i0} the ion gyroradius at the entrance.

Reference 9 already discussed how the response depended on $\hat{\Omega}_{i0}$. It was shown that ion magnetization effects (included the ion azimuthal current) are small in the range $\hat{\Omega}_{i0}\leq O(10)$, which covers most practical applications. In the simulations here, we just take $\hat{\Omega}_{i0}=0.10$.

Reference 9 presented results for a nozzle with $R/R_L\simeq 0.3$ with the turning point of V at $(r,z)=(22,16)$. Here, we analyze mainly simulations for a low divergence-rate nozzle, with $R/R_L\simeq 0.185$ with the turning point of V at $(r,z)\approx(85.2,60.1)$, Fig. 1. Solid black lines in Fig. 2 show the axial variation of main plasma jet magnitudes in that nozzle. The separation between values at the center and border of the jet measures the radial inhomogeneity that develops as the plasma proceeds downstream. It is interesting to compare the axial profiles of this 2D model, with the 'averaged' ones obtained from the simple 1D model[5,14]

$$\hat{R}_V^2(\hat{z})\hat{n}M=M_0,\quad \hat{n}=\mathrm{e}^{\hat{\phi}},\quad M=\sqrt{M_0^2-2\hat{\phi}}. \tag{17}$$

Here $\hat{\phi}$, $\hat{n}$, and M depend only on $\hat{z}$. Potential profiles $\hat{\phi}(\hat{z})$ are obtained from

$$\hat{R}_V^2(\hat{z})\mathrm{e}^{\hat{\phi}}\sqrt{M_0^2-2\hat{\phi}}=M_0. \tag{18}$$

Red lines in Fig. 2 plot the results for the 1D model, which, as expected, lie between those corresponding to the central and border lines of the 2D model. This fact and the relative low radial inhomogeneity for M and $\hat{\phi}$ (about a 25% for $\hat{z}\sim 50$) indicates the validity of the 1D model for predicting the variation of the jet

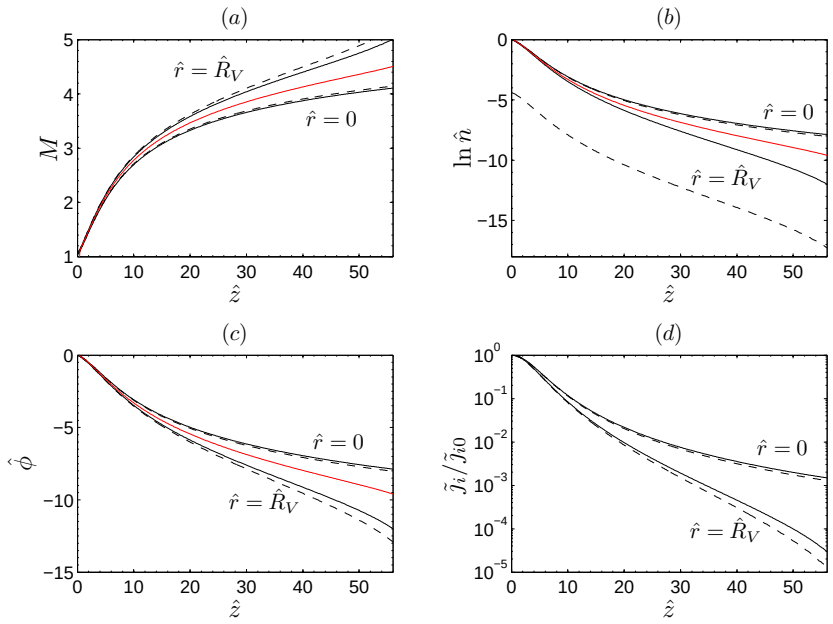

Figure 2. Axial response of main plasma magnitudes at the jet axis and border for the case $R/R_L \simeq 0.185$ and $\hat{\Omega}_{i0} = 0.10$. Solid black lines correspond to a uniform plasma jet ($\sigma = 0$). Red lines correspond to the 1D model of the uniform plasma jet. Dashed lines correspond to a focused plasma jet with $\sigma = 0.99$. In plot (d), ion current densities $j_i(r, z)$ have been normalized to their values at $z = 0$, $j_{i0}(r)$.

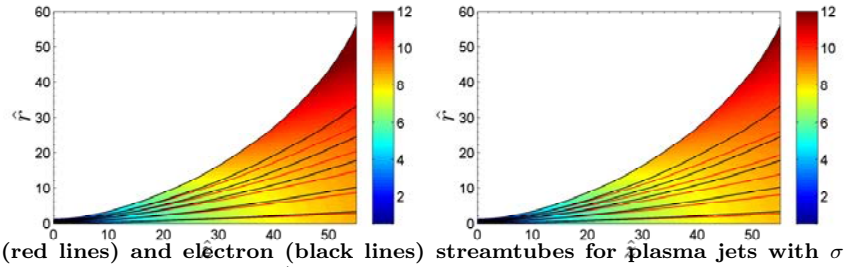

Figure 3. Ion (red lines) and electron (black lines) streamtubes for plasma jets with $\sigma = 0$(a) and 0.99(b). Other parameters are $R/R_L \simeq 0.185$ and $\hat{\Omega}_{i0} = 0.10$. Color maps depict the dimensionless kinetic energy of ions.

kinetic energy, $M^2/2$. However, 2D effects are important for other magnitudes, such as the plasma density and the ion current density, which experience large radial variations, as Fig. 2(b) and 2(d) illustrate.

Figure 3(a) shows the misalignment between the ion and magnetic/electron streamtubes and a color map of the ion velocity for the uniform jet. Figure 4(a) shows how the maximum misalignment angle α_{ei} increases with $\hat{z}$; of course, $\alpha_{ei} = 0$ at the central and border lines. Partially-magnetized ions tend to diverge less than the magnetically-guided electrons. As a consequence, there is more ion current density than electron current density around the jet axis, and a local electric current develops. Since the plasma is current-free globally, the electric current must be negative near the border of the plasma jet. Figures 4(b) to 4(d) illustrate this electric current formation. Observe that the relative current $|\tilde{j}|/\tilde{j}_i$ becomes large at the jet border partially because $\tilde{j}_i$ there is much smaller than at the jet axis. Azimuthal ion currents are not shown; in all cases they are well below a 10% of the longitudinal ion currents.[9] Finally, we do not find any significant difference in the plasma behavior for the high and low divergence-rate nozzles.

IV. Acceleration of a focused plasma jet

The radial structure of a plasma produced inside a cylindrical dielectric vessel of radius R with a strong applied axial magnetic field B_0, parallel to the vessel, consists of a bulk diffusive region and two thin layers:

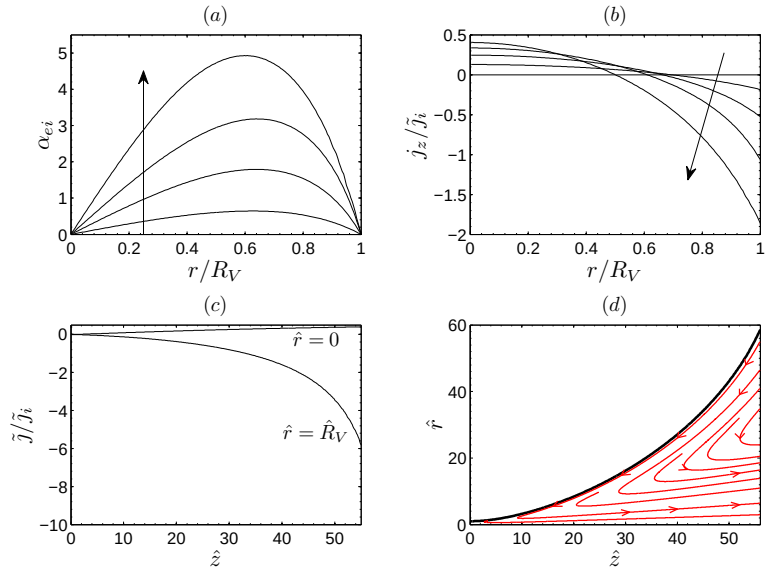

Figure 4. Uniform plasma jet. (a) Misalignment angle (in degrees) between ion an electron streamtubes with z increasing (along the arrow direction). (b) Relative electric current density (along z) at different radial sections. (c) Relative electric current density at the center and the border of the jet. (d) Electric current density lines.

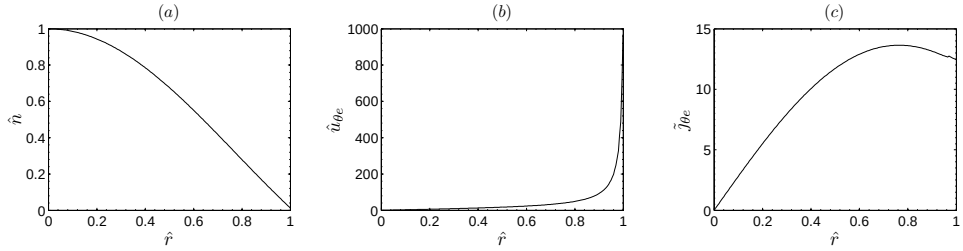

Figure 5. Profiles at the magnetic throat of a focused plasma jet with $\sigma = 0.99$.

a quasineutral inertial layer and the Debye sheaths.[10] Their respective thicknesses are a local electron gyroradius, ℓ_e^* (based on the local change of electron enthalpy), and the local Debye length, λ_D. The hierarchy $\lambda_D \ll \ell_e^* \ll R$ is assumed. The radial plasma behavior in the bulk diffusive region is summarized next for the low-collisionality limit. First, there is a θ-pinch type equilibrium for electrons, which satisfies

$$-en\frac{\partial \phi}{\partial r} \ll enu_{\theta e}B_0 \simeq -T_e\frac{\partial n}{\partial r}. \tag{19}$$

Second, the azimuthal ion velocity is negligible. Third, the plasma radial velocity is very small,

$$u_r \simeq u_{\theta e}/\beta_e, \tag{20}$$

with β_e the electron Hall parameter. Fourth, the ion continuity equation and the above equations yield

$$n(r) = n_0 J_0\left(a_0\frac{r}{R}\right), \qquad u_{\theta e}(r) = \frac{T_e a_0}{eB_0 R}\frac{J_1(a_0 r/R)}{J_0(a_0 r/R)}, \tag{21}$$

with J_0 and J_1 Bessel functions of first kind, and $a_0 \simeq 2.405$, the first zero of J_0. Thus, the Hall current satisfies

$$j_{\theta e}(r) = en_0\frac{T_e a_0}{eB_0 R}J_1\left(a_0\frac{r}{R}\right).$$

Fifth, at the transition to the thin inertial layer, $u_{\theta e}$ is of the order of the electron thermal velocity, $c_e = \sqrt{T_e/m_e}$, and the Hall current is

$$j_{\theta e} \simeq a_0 J_1(a_0)\frac{en_0 c_s^2}{R\Omega_{i0}}, \tag{22}$$

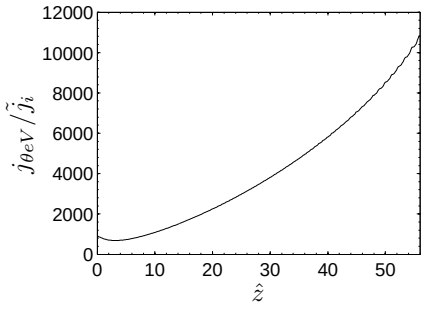

Figure 6. Variation along the nozzle of the relative Hall current at the border of the focused plasma jet.

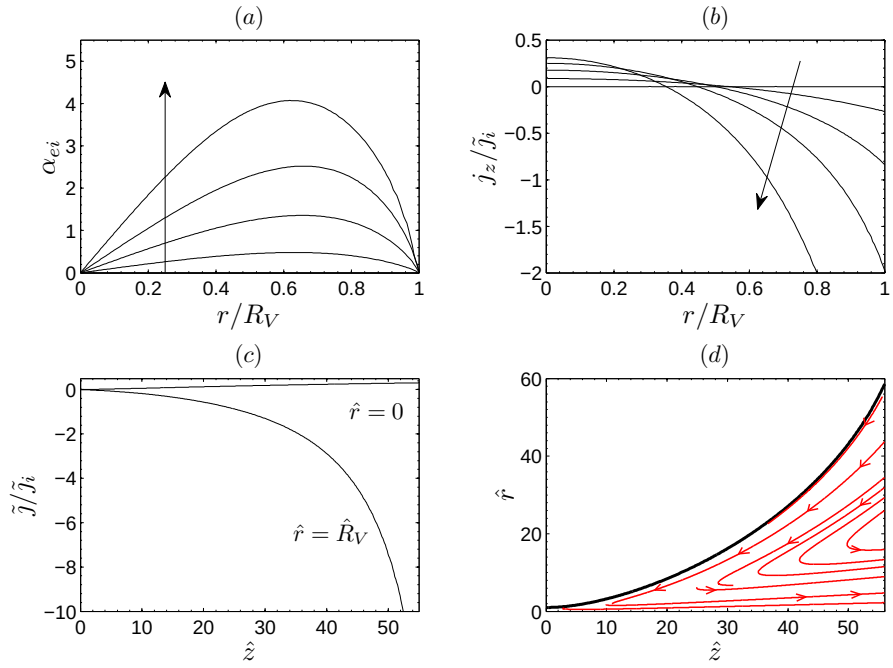

Figure 7. Same as Fig. 4, for the focused plasma jet.

with $a_0 J_1(a_0) \simeq 1.25$.

Boundary conditions at the magnetic throat of our model, consistent with the above plasma behavior, the collisionless limit, the hierarchy $\lambda_D \ll \ell_e^* \ll R$, and a current-free plasma, are Eqs. (14), (15), and

$$\hat{\phi}(\hat{r},0)=0, \quad \hat{n}(\hat{r},0)=J_0(a_0\sigma\hat{r}), \quad \hat{u}_{\theta e}(\hat{r},0)=\frac{a_0}{\hat{\Omega}_{i0}}\frac{J_1(a_0\sigma\hat{r})}{J_0(a_0\sigma\hat{r})}, \tag{23}$$

with

$$1-\sigma \sim \hat{\Omega}_{i0}^{-1}\sqrt{m_e/m_i},$$

in order that $u_{\theta e} \sim c_e$ at the jet border. Figure 5 plots the profiles of $\hat{n}_e$, $\hat{u}_{\theta e}$, and $\hat{j}_{\theta e}$ for $\sigma = 0.99$. One has $\hat{n}_e$ and $\hat{u}_{\theta e}\hat{\Omega}_{i0}$ of order one except near the jet border. Observe that the azimuthal electron current at the throat is $\hat{j}_{\theta e}(r,0) = J_1(a_0\sigma\hat{r})a_0/\hat{\Omega}_{i0}$.

The dashed lines of Fig. 2 show the acceleration of the focused jet along the nozzle. Results for M and ϕ are very close to the uniform jet case and are well approximated by the 1D model. Obviously, the main differences between the uniform and focused jet cases are in the radial profiles of the plasma density and related magnitudes. Figure 6 shows the variation along the nozzle of the relative Hall current at the jet border (where it is maximum). The plotted magnitude increases proportionally to $R_V(z)/M_V(z)$.

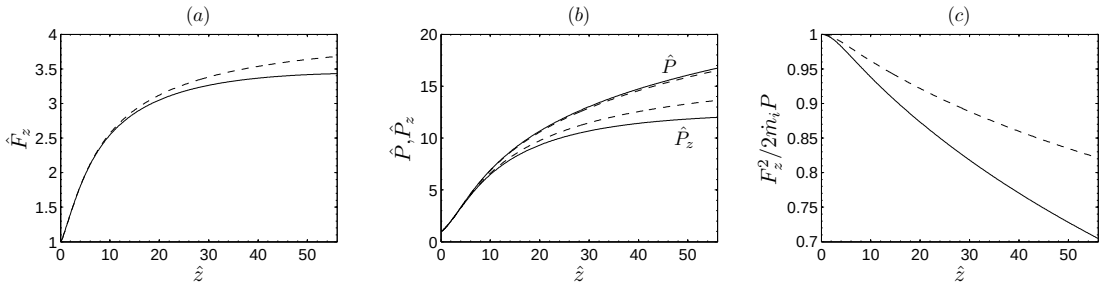

Figure 8. Variation along the nozzle of (a) ion axial momentum flow, (b) ion axial and total energy flow, and (c) nozzle efficiency, for the uniform (solid) and the focused (dashed) plasma jets.

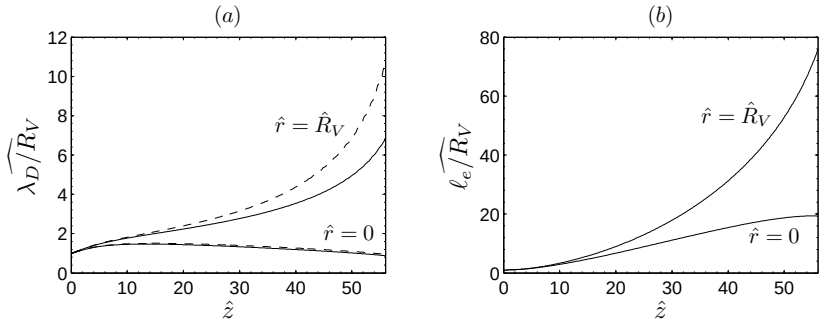

Figure 9. Variation along the nozzle of the relative (a) quasineutrality and (b) magnetic-guiding parameters, for the uniform (solid) and the focused (dashed) plasma jets.

The comparison of Figs. 3(a) and 3(b), and Figs. 4 and 7, show that the differences in ion-electron misalignment and local electric current between the uniform and focused jets are not very significant. The much larger radial density drop for the focused jet produces a larger negative electric current at the jet border.

The radial expansion of the plasma jet reduces the thrust efficiency of the ideal nozzle expansion. The efficiency of the ion acceleration process along the nozzle is measured by

$$\eta_{noz}(z) = \frac{F_z^2}{2\dot{m}_i P}, \tag{24}$$

with $\dot{m}_i$ the (constant) mass flow, $F_z(z)$ the axial ion momentum flow, and $P(z)$ the flow of ion kinetic energy; the flow axial kinetic energy, $P_z(z)$, is a useful magnitude too. Figure 8 plots these magnitudes for the two plasma jets considered here. The most relevant result is the much better performance of the focused jet due to the concentration of most of the plasma near the axis, where radial forces are small.

Figure 9 plots the evolution of the parameters measuring the validity of plasma quasineutrality and electron magnetic guiding. The wide hat on the variables means that all curves are normalized to their values at $z = 0$. Observe that for the focused jet $\lambda_D(R, 0) \gg \lambda_D(0, 0)$. Near the throat, one has $\lambda_D(R_V)/R_V \propto M^{1/2}$, but far downstream it increases faster because of the larger radial rarefaction of the plasma. For the magnetic guiding parameter one has $\ell_e/R_V \propto R_V^{-1} B^{-1} \propto R_V$.

V. Detachment of the focused plasma jet

The detachment of this collisionless plasma can be achieved via an induced magnetic field that stretches axially the magnetic tube containing the plasma[8,15] or via electron inertia effects that detach effectively the plasma jet from the guiding magnetic tube.[6] Although the model studied here cannot simulate the plasma detachment, it allows to assess whether any of the above mechanisms is relevant. The first important point, as we will see next, is that both mechanisms depend on the presence of a Hall current, so they can develop only for the focused plasma jet case.

Once the electric current density is known, the induced magnetic field, $\boldsymbol{B}^\star$, is computed from $\nabla \times \boldsymbol{B}^\star =$

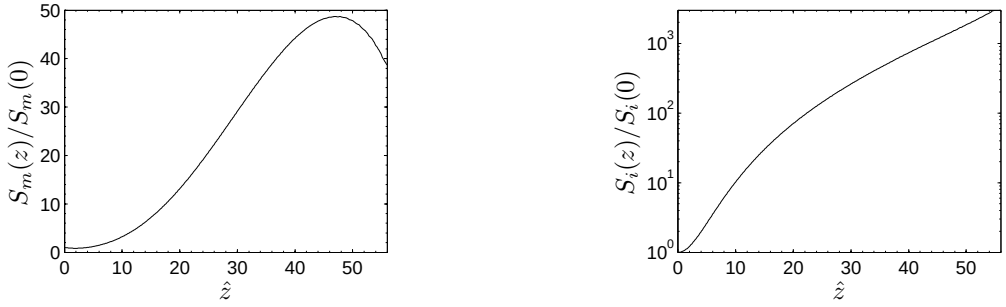

Figure 10. Increase along the nozzle of the magnetic-detachment and inertial-detachment parameters along the nozzle for the focused plasma jet.

$\mu_0 \boldsymbol{\jmath}$. Thus, the azimuthal Hall current induces a longitudinal magnetic field satisfying

$$\frac{\partial B_r^\star}{\partial z} - \frac{\partial B_z^\star}{\partial r} = \mu_0 j_\theta, \quad \frac{1}{r}\frac{\partial r B_r^\star}{\partial r} + \frac{\partial B_z^\star}{\partial z} = 0. \tag{25}$$

An estimate of the longitudinal induced field is given by

$$B_z^\star \sim \mu_0 j_{\theta e} r \propto n r^2 \sim M^{-1}. \tag{26}$$

Then, the *magnetic detachment parameter*, S_m, can be defined as the ratio between the induced and the applied field,

$$S_m(z) = \mu_0 j_{\theta e} r B^{-1}\big|_{r=R_V(z)}. \tag{27}$$

Using Eq. (22), at the nozzle throat one has

$$S_m(0) \approx 1.25 c_s^2/c_A^2,$$

with $c_A = B/\sqrt{\mu_0 m_i n}$ the Alfven velocity, based on the guiding field. Figure 10(a) depicts $S_m(z)/S_m(0)$, which starts varying proportionally to $R_V(z)^2 M^{-1}$, according to Eq. (26), but then it stops growing because of the large plasma rarefaction at the jet border. Therefore, for the simulated case, the induced magnetic field is relevant only if $S_m(0) > O(10^{-2})$, which is not the case for the plasmas of Table 1.

The longitudinal electric current induces an azimuthal magnetic field, but this is really small. A simple estimate yields

$$B_\theta^\star / B_z^\star \sim \jmath / j_{\theta e} \ll 1. \tag{28}$$

Plasma detachment via electron inertia was discussed by Hooper.[6] The relevant term is the electron inertia in the azimuthal electron equation, which leads to an equation for the conservation of the electron axial angular momentum, similar to Eq. (5) for ions,

$$r m_e u_{\theta e} - e\psi = D_e(\psi_e), \tag{29}$$

with, ψ_e the electron streamfunction. In the massless limit, the first term on the left is negligible and Eq. (29) reduces to the biunivocal relation between ψ_e and ψ. Inertial effects become important when the first term in Eq. (29) becomes of the order of the second one. Thus, the *inertial detachment parameter* is

$$S_i(z) = r m_e u_{\theta e} (e\psi)^{-1}\big|_{r=R_V(z)}. \tag{30}$$

At the nozzle throat one has

$$S_i(0) \approx 2\ell_e/R.$$

Figure 10(b) plots $S_i(z)/S_i(0)$. Since $\psi_V = \text{const}$ and $u_{\theta e} \propto r$, $S_i(z)$ increases proportionally to the nozzle radial area, i.e. $\propto R_v(z)^2$.

Since $S_i(z)/S_i(0)$ increases much more than $S_m(z)/S_m(0)$, and Table 1 shows than $S_m(0)/S_i(0)$ is not likely to be large for a focused plasma jet, detachment via electron inertia seems to be more likely, at least for the plasma jets considered here.

VI. Summary

A 2D model of plasma acceleration in a divergent magnetic nozzle has been applied to a focused plasma jet and compared to the case of a uniform plasma jet. For both cases, axial acceleration is similar, the ion azimuthal drift is negligible, and local electric currents develop. The nozzle efficiency is higher for the focused plasma jet due to the concentration of most of the plasma around the nozzle axis.

For a focused plasma jet, the Hall current density that creates the magnetic force sustaining the radial density gradient increases downstream and is able to develop both an induced magnetic field and azimuthal inertia effects on electrons, which are the two envisaged detachment mechanisms in a collisionless plasma. The electron inertia mechanism seems a stronger one for the plasmas considered in this work.

Finally, it is worth to mention that in all cases the acceleration of our simple plasma is quasineutral and the size of the ambipolar electric field depends on the plasma temperature and the geometrical lengths of the nozzle. Some authors have claimed the formation of a current-free (non-neutral) double layer in a plasma expanding in a magnetic nozzle inside a vacuum chamber.[16–18] Ahedo and Martínez-Sánchez have shown that, when the plasma expands into vacuum, the formation of such double layer requires the presence of two electron populations with disparate temperatures.[14,19]

Acknowledgements

This work was supported by the Ministerio de Ciencia e Innovación of Spain (Project ESP2007-62694) and the European Community (Grant 218862).

References

[1]G. Krülle, M. Auweter-Kurtz, and A. Sasoh, J. Propulsion and Power **14**, 754 (1998).

[2]S. A. Cohen, X. Sun, N. Ferraro, E. E. Scime, M. Miah, S. Stange, N. Siefert, and R. Boivin, IEEE Transactions on Plasma Science **34**, 792 (2006).

[3]A. Arefiev and B. Breizman, Physics of Plasmas **11**, 2942 (2004).

[4]D. Courtney and M. Martínez-Sánchez, Diverging Cusped-Field Hall Thruster, in *30th International Electric Propulsion Conference, Florence, Italy*, IEPC-2007-39, Electric Rocket Propulsion Society, Fairview Park, OH, 2007.

[5]S. A. Andersen, V. O. Jensen, P. Nielsen, and N. D'Angelo, Phys. Fluids **12**, 557 (1969).

[6]E. B. Hooper, Journal of Propulsion and Power **9**, 757 (1993).

[7]A. Arefiev and B. Breizman, Physics of Plasmas **12**, 043504 (2005).

[8]C. A. Deline, R. D. Bengtson, B. N. Breizman, M. R. Tushentsov, J. E. Jones, D. G. Chavers, C. C. Dobson, and B. M. Schuettpelz, Physics of Plasmas **16**, 033502 (2009).

[9]E. Ahedo and M. Merino, Two-dimensional plasma acceleration in a divergent magnetic nozzle, in *44th Joint Propulsion Conference, Hartford, CT*, AIAA 2009-5361, American Institute of Aeronautics and Astronautics, Washington DC, 2008.

[10]E. Ahedo, Cylindrical model of a helicon-generated plasma, in *31th International Electric Propulsion Conference, Ann Arbor, Michigan, USA*, IEPC 2009-193, Electric Rocket Propulsion Society, Fairview Park, OH, 2009.

[11]J. Jackson, *Classical Electrodynamics*, Wiley, New York, 1999.

[12]M. Abramowitz and I. Stegun, *Handbook of Mathematical Functions*, Dover, New York, 1965.

[13]M. Zucrow and J. Hoffman, *Gas dynamics* , Wiley, New York, 1976.

[14]E. Ahedo and M. Martínez-Sánchez, The Role Of Current-Free Double-Layers In Plasma Propulsion, in *44th Joint Propulsion Conference, Hartford, CT*, AIAA 2008-5005, American Institute of Aeronautics and Astronautics, Washington DC, 2008.

[15]R. Winglee, T. Ziemba, L. Giersch, J. Prager, J. Carscadden, and B. R. Roberson, Physics of Plasmas **14**, 063501 (2007).

[16]C. Charles and R. Boswell, Applied Physics Letters **82**, 1356 (2003).

[17]S. A. Cohen, N. S. Siefert, S. Stange, R. F. Boivin, E. E. Scime, and F. M. Levinton, Physics of Plasmas **10**, 2593 (2003).

[18]X. Sun, A. Keesee, C. Biloiu, E. Scime, A. Meige, C. Charles, and R. Boswell, Physical Review Letters **95**, 025004 (2005).

[19]E. Ahedo and M. Martínez-Sánchez, 'Theory of a stationary current-free double-layer in a collisionless plasma' to be published in Physical Review Letters (2009).